

UNIVERSITY OF PENNSYLVANIA

# **Use of Compton Backscatter X-ray Imaging in Agriculture**

by

John Buglione

A thesis submitted in partial fulfillment for the  
degree of Masters of Engineering

in  
Robotics  
School of Engineering and Applied Science

May 2016

Camillo J. Taylor

**Graduate Group Chair & Thesis Advisor**

*“I like fruit baskets because it gives you the ability to mail someone a piece of fruit without appearing insane. Like, if someone just mailed you an apple you’d be like, “huh? What the hell is this?” But if it’s in a fruit basket you’re like, “this is nice!”*

Demetri Martin

## *Acknowledgements*

Firstly I would like to thank my family for supporting me throughout my time at school.

I would also like to thank Dr. C.J. Taylor, Dr. Vijay Kumar, and all of the members of the Kumar Lab Ag Bio group for their continued help throughout this project. Finally, I would like to thank Jim Schupp of the Penn State Fruit Research and Extension Center, Driscoll Strawberries, and Lipman Produce for use of their facilities throughout the course of this project.

UNIVERSITY OF PENNSYLVANIA

## *Abstract*

Robotics

School of Engineering and Applied Science

Masters of Engineering

by [John Buglione](#)

Precision agriculture, specifically yield estimates, provide economic and environmental benefits to farm operators. Many automated fruit yield estimation techniques rely on RGB cameras or other imaging techniques in which fruit obscuration due to leaf cover can make getting an accurate estimate of fruit count difficult. This paper explores the use of Backscatter X-Ray imaging as an alternative imaging modality with foliage penetrating properties. Example scans are displayed and a method of estimating fruit yield of trellis grown apple trees is proposed.

# Contents

<b>Acknowledgements</b>	ii
<b>Abstract</b>	iii
<b>List of Figures</b>	vi
<b>Abbreviations</b>	vii
<b>Physical Constants</b>	viii
<b>Symbols</b>	ix
<b>1 Introduction</b>	1
1.1 Precision Agriculture . . . . .	1
1.2 Specialty Crops . . . . .	2
1.3 Measurement Methods . . . . .	3
1.4 Imaging Modalities . . . . .	4
<b>2 Background of Imaging Methodology</b>	5
2.1 Overview . . . . .	5
2.2 Compton Shift . . . . .	6
2.3 X-ray Generation . . . . .	7
2.4 Generating an Image . . . . .	10
<b>3 Experimental Setup</b>	11
3.1 Compton Backscatter Imaging Equipment . . . . .	11
3.1.1 Unit Internals . . . . .	11
3.1.2 ModBX . . . . .	12
3.1.3 Mini-Z . . . . .	13
3.2 Target Crops . . . . .	13
<b>4 Imaging</b>	15
4.1 Apples . . . . .	15
4.1.1 Axial Scan . . . . .	16
4.1.2 Radial Scan . . . . .	18
4.2 Strawberries . . . . .	19
4.3 Tomatoes . . . . .	19

<b>5 Sample Analysis of Image</b>	<b>22</b>
5.1 Process overview . . . . .	23
5.1.1 Filtering Images . . . . .	23
5.1.2 Processing Using Structured Elements . . . . .	24
5.1.3 Image Segmentation . . . . .	26
5.1.4 Using Path Planning to Locate the Trunk . . . . .	28
5.1.5 Determining Fruit Yield . . . . .	30
<b>6 Conclusions</b>	<b>31</b>
6.1 Overview . . . . .	31
6.2 Conclusions . . . . .	31
6.3 Future Work . . . . .	32
<b>A Image Processing Pseudocode</b>	<b>33</b>
<b>Bibliography</b>	<b>36</b>

# List of Figures

2.1	Compton Scatter . . . . .	7
2.2	X-Ray Tube [1] . . . . .	8
2.3	Typical Spectrum for Tungsten-Target X-Ray Tube . . . . .	9
3.1	Backscatter X-Ray Imager Chopper Wheel . . . . .	12
3.2	AS&E Mod BX Scanner and Scanner Being Used in Middle Scan Mode .	13
3.3	AS&E Mini-Z Scanner . . . . .	13
4.1	ModBX Scanner Prepared for a Radial Scan . . . . .	16
4.2	Axial Scan and Photograph of Trellis Planted Apple Trees . . . . .	17
4.3	Radial Scan of Trellis Planted Apple Trees . . . . .	18
4.4	Scan and Photograph of Ground Planted Strawberries . . . . .	19
4.5	Photograph of Trellis Planted Tomatoes. Courtesy of Lipman Produce. .	20
4.6	Vertical Scan of Tomato Plant . . . . .	20
4.7	Horizontal Scan of Tomato Plants . . . . .	21
5.1	Scan of Apple Tree from ModBX Backscatter X-Ray Imager . . . . .	23
5.2	Scan After Application of Median Filter . . . . .	24
5.3	Adaptive Histogram Equalization . . . . .	24
5.4	Morphological Opening . . . . .	25
5.5	Second Morphological Opening . . . . .	26
5.6	Image After Intensity Adjustment . . . . .	26
5.7	Binarized Image . . . . .	27
5.8	Binarized Image with Objects Removed . . . . .	27
5.9	Trunk Boundary . . . . .	28
5.10	Optimal Path Through Trunk . . . . .	29
5.11	Scan With Trunk Removed . . . . .	30

# Abbreviations

**USDA** United States Department of Agriculture

**ROI** Return On Investment

**AMS** Agricultural Marketing Service

**AS&E** American Science and Engineering

# Physical Constants

Speed of Light	$c = 2.997\ 924\ 58 \times 10^8\ \text{ms}^{-\text{s}}$
Dirac's Constant	$\hbar = 6.582\ 119\ 514 \times 10^{-16}\ \text{evS}$
Electron Rest Mass	$m_e = 9.109\ 382\ 15 \times 10^{31}\ \text{kg}$

# Symbols

$p_0$	Initial Momentum
$K_0$	Initial Kinetic Energy
$\omega$	Frequency
$E$	energy
$\lambda$	Wavelength
$v$	Velocity
$Z$	Z Mean Atomic Number

# **Chapter 1**

## **Introduction**

This thesis provides an introduction to the use of Compton Backscatter X-ray Imaging in precision agriculture. We will explore the use of this imaging technique on specialty crops and some sample results. A method of estimating crop yield using backscatter X-Ray imaging will also be proposed.

### **1.1 Precision Agriculture**

Precision agriculture as defined by the USDA is “a management system that is information and technology based, is site specific, and uses one or more of the following sources of data: soils, crops, nutrients, pests, moisture, or yield, for optimum profitability, sustainability and protection of the environment.” [2] This paper is interested in yield monitoring systems; ways of spatially and temporally measuring agricultural yield, specifically in specialty crops. Using information collected by yield monitoring systems, growers can make informed decisions about the management of crops on a farm. The fine spatial resolution of modern yield monitoring systems allow growers to use targeted

irrigation, fertilization, and pest management schemes in order to optimize the output of their farm based on the capability of their plots of land. Precision agricultural techniques also allow growers to be more environmentally conscious when making decisions regarding crop care via the ability to identify land that should be taken out of production due to environmental concerns.

As well as environmental benefits, precision agriculture can provide substantial economic benefit to farmers. The ability to improve crop yields along with the decreased costs associated with better targeted irrigation and fertilization provides a financial benefit to farmers. Technology involved in precision agricultural practices can be a large initial investment for crop growers. In spite of this, in some cases the use of precision agriculture has been able to provide farmers with a ROI in as little as 2-5 years from the initial financial outlay. [3]

## 1.2 Specialty Crops

Specialty crops, contrary to what their name may imply, make up a large proportion of US agriculture. Recently specialty crops have come to make up thirty to forty percent of the total value of US crops. [4] As defined by AMS, specialty crops are “fruits, vegetables, tree nuts, dried fruit, and horticultural and nursery crops, including floriculture.” [5] In this paper we are mainly interested in horticulture, ”the science and art of producing, improving, marketing, and using fruits, vegetables, flowers, and ornamental plants.” [6] The crop discussed in most detail in this paper is trellis grown apple trees. Ground grown strawberries and trellis grown tomatoes will also be investigated.

### 1.3 Measurement Methods

There are various methods of determining crop yield in specialty crops. Currently, many growers use a method of yield estimation that involves a manual count of the agricultural product (fruits, nuts, vegetables...) on an individual plant and extrapolating this count in order to get an estimate of the overall yield of the crop. [7]

In some cases estimating yield is more a mix of art and science than pure science. An example of this can be seen in one current way that apple yield is estimated. Experienced field scouts are sent into orchards in order to take a manual count of the number of apples on a tree. This count can be obtained by exhaustively counting the total number of apples on an individual plant or by counting the number of fruit on a series of limbs across a few trees. This count is then extrapolated in order to estimate the number of fruit in the orchard. Once the fruit count is obtained, the average size of the fruit on the trees must be estimated. This can be obtained by sampling the size of individual fruit across a series of plants. These two estimates are then compared to models developed by monitoring specific varieties of trees for a number of years in order to estimate the overall yield of the orchard. [7] These yield estimates are not very robust, given that not all cultivars of apple are modeled for every growing region.

There are also ways of using remote sensing in order to spatially determine crop yield across a farm. These methods focus on using satellite imagery in combination with ground samples (soil, moisture, ...) in order to estimate stress on an area of plants. [8]

The method of measurement that this paper is interested in is a direct estimate of the agricultural product across a group of plants. An image of a plant is generated using X-Ray backscatter imaging and fed into computer software that identifies various aspects of the image. Once all of the aspects are identified a spatial estimate of the crop yield

can be calculated. This provides a yield estimate with high spacial resolution necessary for precision agriculture.

## 1.4 Imaging Modalities

While the remote imaging method of yield estimation discussed in 1.3 can provide a count across a plot, this count is coarse. One fine yield estimation method currently being researched is imaging in the visible spectrum with an RGB camera and counting the fruit visible in the images. [9] While this method provides promising results, the obscuration of the fruit by the foliage of the plants can cause problems when trying to estimate the number of fruit on an individual plant. Thermal cameras have also been used to estimate fruit count, but similarly to RGB cameras suffer from problems due to obscuration. [10]

## Chapter 2

# Background of Imaging

## Methodology

Due to the issues of obscuration discussed in [1.4](#), Compton Backscatter X-Ray was chosen as an imaging technology that would provide foliage penetration. This allows crop yields to be estimated without needing to account for fruit obscured by leafage.

### 2.1 Overview

The basis of Compton Backscatter X-Ray imaging is the Compton Scattering effect. Compton Scattering is “the scattering of a high-energy photon with loss of energy that occurs in the Compton effect.” [\[11\]](#) By exciting materials with X-Ray radiation and measuring the scattered photons, an image can be constructed that is representative of the materials present in the imaging field scanned by the X-Ray beam. The resulting image is similar to a traditional transmission X-Ray image, but does not require the use of a detector situated behind the target being imaged.

## 2.2 Compton Shift

The primary physical property that makes Compton Backscatter imaging possible is the Compton Shift effect. Compton Shift occurs when a primary light quantum  $k_0$  collides with a free electron [2.1](#) (assumed to be initially at rest).

$$p_0 = 0, E_0 = \mu = mc^2 \quad (2.1)$$

When these two particles collide the electron recoils. Due to conservation of momentum when light quanta interact with free electrons, the electron absorbs some momentum and energy from the initial quantum. [2.2](#)

$$p = k_0 - k \quad (2.2)$$

$$E + k = k_0 + \mu \quad (2.3)$$

Because of [2.2](#) and [2.3](#) there is a shift in the frequency of the quanta. Taking into account the relativistic energy-momentum relation [2.4](#) and the angle  $\theta$  between  $k_0$  and  $k$  we arrive at a formula describing the frequency shift between the two quanta. [2.5](#)

$$p^2 = E^2 - \mu^2 \quad (2.4)$$

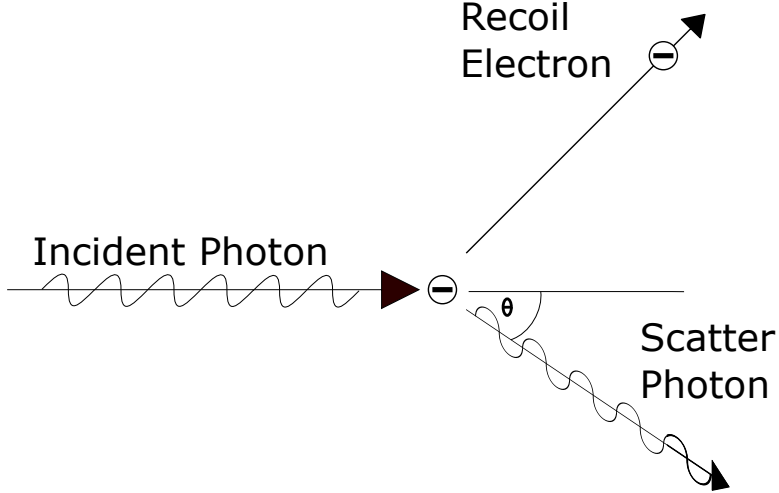
$$k = \frac{k_0\mu}{\mu + k_0(1 - \cos\theta)} \quad (2.5)$$

By using the relationship between wavelength and the frequency of the particle [2.6](#) we can arrive at a formula describing the shift in wavelength of the quantum. [2.7](#)

$$\lambda = \frac{\hbar c}{k} \sim \frac{\hbar c}{k} \equiv \lambda_0 \quad (2.6)$$

$$\lambda - \lambda_0 = \frac{\hbar}{m_e c} (1 - \cos \theta) \quad (2.7)$$

FIGURE 2.1: Compton Scatter

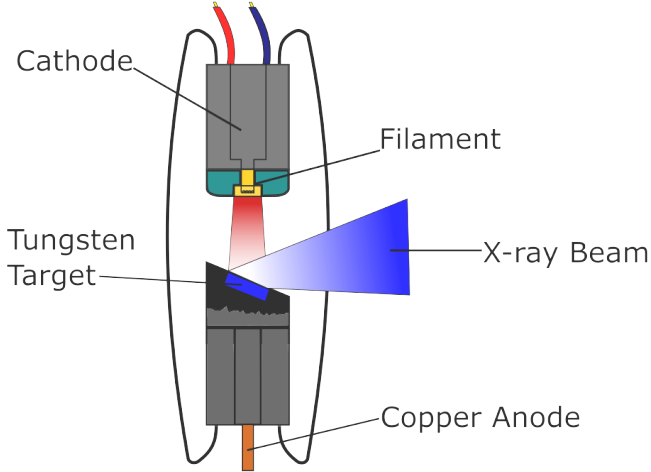


Compton Scattering is a specific case of quantum electrodynamic scattering described by the Klein-Nishina formula, which gives the differential cross section of photons scattered from a free electron, that occurs at higher frequencies(X and  $\gamma$  rays).

### 2.3 X-ray Generation

The Compton Backscatter X-Ray imager used in this thesis generates X-Rays using an X-Ray tube. The tube generates X-Rays through an effect known as Bremsstrahlung as well as K-shell emission.

FIGURE 2.2: X-Ray Tube [1]



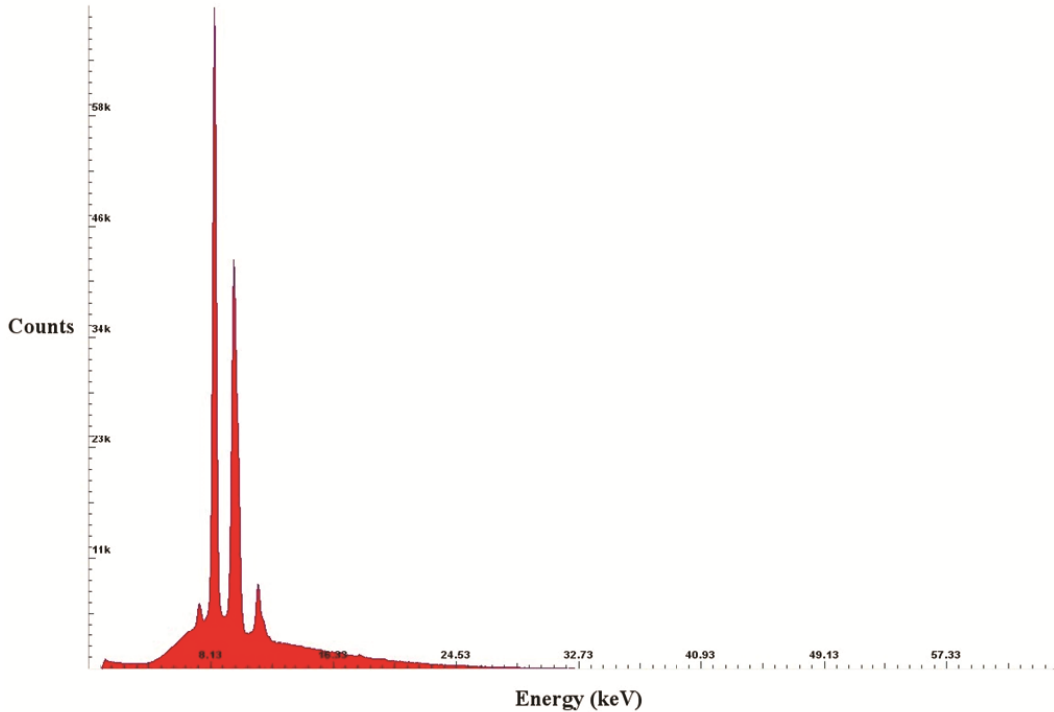
Within the X-Ray tube there is an electron gun that fires a beam of electrons at a heavy metal target, in many cases tungsten. When these electrons collide with the tungsten target they quickly decelerate and emit electromagnetic radiation. When the electrons are accelerated to a high enough energy they will emit radiation in the form of X-rays. The radiative cross section  $\chi(\omega)$ , which represents the likelihood of a such a scattering event emitting Bremsstrahlung radiation, is shown in 2.8 below. [12].

$$\chi(\omega) = A \left[ \ln \frac{2\lambda\gamma^2 M v^2}{\hbar\omega} - \frac{13}{12} \right], A = \frac{16}{3} \frac{Z^2 e^2}{c} \left( \frac{z^2 e^2}{Mc^2} \right)^2 \left( \frac{c}{v} \right)^2 \quad (2.8)$$

K-Shell emission, also known as characteristic radiation, occurs when an electron in the outer shell of an atom drops into the atom's inner shell. [13] High energy X-Rays can knock electrons out of the inner shell of an atom. This leaves an electron hole can then be filled by an electron from one of the atom's outer shells. When the higher energy electron drops shells, the difference in energy between the outer and inner shells is emitted as an X-ray photon. Different materials have unique K-Shell emission signatures.

Both Bremsstrahlung and K-Shell radiation can be seen in the sample spectra from a tungsten anode X-Ray tube in figure 2.3.

FIGURE 2.3: Typical Spectrum for Tungsten-Target X-Ray Tube



Bremsstrahlung radiation makes up the smooth base curve of the emission spectrum while K-Shell radiation forms the prominent peaks.

Due to the way that X-Ray tubes generate X-Ray radiation, both the frequency and the number of X-Ray photons that are emitted from the tube can be altered. Increasing the current through the cathode heating filament will increase the temperature of the cathode itself, allowing more electrons to be ejected from the cathode and collide with the anode, thus increasing the overall number of scattering events and therefore the number of scattered X-Ray photons. By changing the voltage between the cathode and anode, the velocity and therefore energy of the electrons that collide with the anode can be

altered. As can be seen in [2.8](#) this will change the overall spectra of the Bremsstrahlung radiation emitted from the anode.

## 2.4 Generating an Image

In order to generate an image using Compton Backscatter X-Rays, a thin beam of X-Rays is scanned along the object that is being imaged. The X-Rays photons collide with free electrons in the object and are scattered. Due to Compton shift, these scattered photons are of decreased wavelength and can be detected using sensors in the imaging device. The detected signal is then processed using various signal processing techniques and used to construct an image. [\[14\]](#) Objects with different average atomic masses ( $Z$  number) will appear as differently on the resulting image, due to different probability of scatter occurring.

# Chapter 3

## Experimental Setup

### 3.1 Compton Backscatter Imaging Equipment

Two different imaging systems were used over the course of this thesis. Both units, sourced from AS&E, operate using the same basic principles. The key differences between the two involve the size of the units, the amount and energy of X-Rays that the units emit, and the size of the area that can be imaged using each unit.

#### 3.1.1 Unit Internals

At their cores, both units have an X-Ray tube enclosed within a chopper wheel. [3.1](#) This chopper wheel takes the X-Ray radiation emitted by the tube and directs it into a pencil-width beam that is vertically scanned. The vertically scanned beam is moved horizontally along a target by either rotating or translating the device, and as a result a moving point on the target is illuminated by X-Ray radiation.

Due primarily to the Compton effect discussed earlier, the X-Ray radiation from the beam interacts with electrons in the target via Compton Scattering and lower energy photons are emitted. These scattered photons are then detected using sensors in the front of the unit. Due to the probabilistic nature of the scattering effect, different amounts of detected scattering can be related to the density (Z number) and thickness of the objects being scanned. Thus, the signal from these detectors can be reconstructed into an image that is representative of the object being scanned. [15]

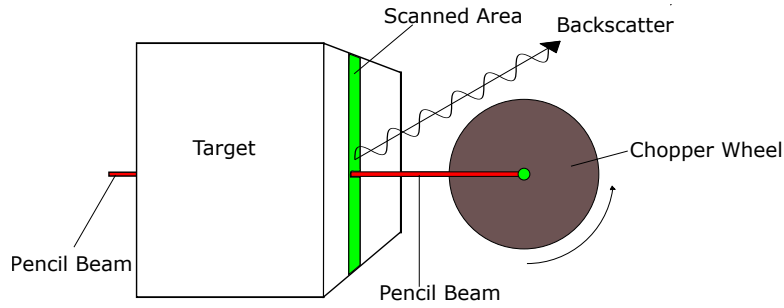


FIGURE 3.1: Backscatter X-Ray Imager Chopper Wheel

### 3.1.2 ModBX

The ModBX unit is an experimental scanner mounted on a mechanical turret. It can be used to take both axial scans using the in-built turret; or the entire scanner can be moved across a target in order to take a linear scan. The scanner has a variable scan time between 15 and 120 seconds and an 140keV, 550W X-Ray tube. The ModBX scanner has three scan heights that it can select; low, middle, and high. The low scan height directs the scanning beam to the area immediately in front of and below the scanner, the middle scan directs the beam towards the front of the scanner, and the high scan directs the scan immediately in front and below the scanner.

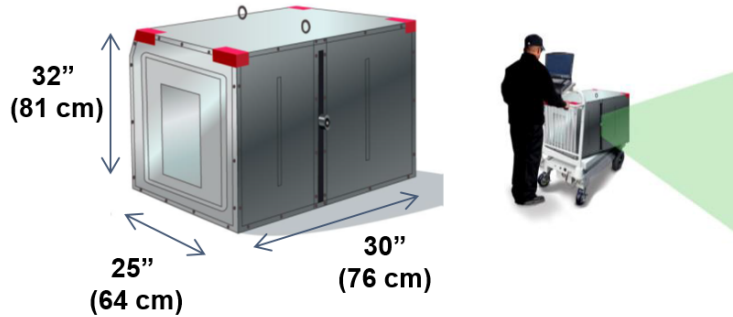


FIGURE 3.2: AS&E Mod BX Scanner and Scanner Being Used in Middle Scan Mode

### 3.1.3 Mini-Z

The Mini-Z scanner unit is a miniaturized version of the chopper wheel backscatter X-Ray scanner described in [3.1.1 \[16\]](#). It is handheld and is manually swept across the target. The scanner has a variable scan time between 5 and 45 seconds and an 70keV, 10W X-Ray tube. The Mini-Z scanner has a nominal scan speed of 15cm/sec. [\[17\]](#)



FIGURE 3.3: AS&E Mini-Z Scanner

## 3.2 Target Crops

Three different crops were scanned using Compton Backscatter X-Ray imaging. These crops were trellis grown apples, ground grown strawberries, and trellis grown tomatoes.

The details of this process are discussed in detail in chapter 4.

# Chapter 4

## Imaging

### 4.1 Apples

Trellis grown apples at an orchard in Biglerville, PA were scanned using the ModBX scanner described previously. [3.1.2](#) The trees were scanned in two different ways. Firstly, the scanner was situated about 3.5m from the base of the trees and was allowed to axially scan a subsection of the row of trees using the turret built into the base of the scanner. Next, the scanner was moved parallel to the row of trees and allowed to radially scan a subsection of the row. The tree crowns were about 3m from the ground and the scanner was mounted to the tines of a tractor and leveled.



FIGURE 4.1: ModBX Scanner Prepared for a Radial Scan

#### 4.1.1 Axial Scan

Due to the geometry of the projected beam when performing an axial scan, there is a slight barrel distortion effect that occurs, in which objects at the far left and right of the scan appear smaller than objects near the center. Also, due to the strength of the X-Ray beam incident upon objects decreasing with increased distance between objects and the X-Ray emitter, distant objects appear more dimly in the images than objects closer to the scanner.



FIGURE 4.2: Axial Scan and Photograph of Trellis Planted Apple Trees

Due to the higher apparent density of the apples and trunk as compared to empty areas containing mostly foliage, these appear as light areas on the image. As can be seen in figure 4.3 many of the apples that are obscured in the photograph are clearly visible in the Backscatter X-Ray scan. There is also a horizontal line dividing the top and bottom half of the image. This is due to the way that images were reconstructed from the ModBX's middle and low scan settings. 3.1.2

#### 4.1.2 Radial Scan

As discussed earlier, axial scans performed using the Mod BX scanner suffer from distortion and detection issues involving the increased distance that objects at the edges of the scan are from the scanner. One way to alleviate these problems is by moving the scanner linearly along the target that is being scanned. The ModBX scanner was mounted on a tractor so that the scanning beam was emitted perpendicularly to the tractor's direction of movement. The tractor then moved along the row of apples as the scanner was running in order to generate a radial push broom scan.

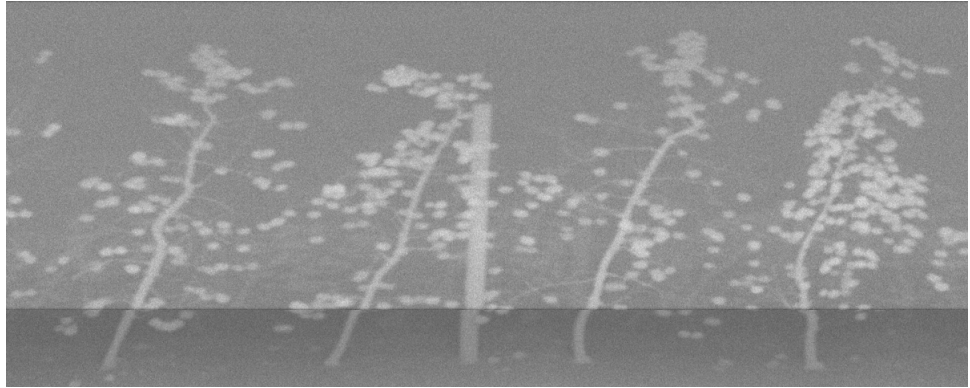


FIGURE 4.3: Radial Scan of Trellis Planted Apple Trees

As can be seen by looking at the bases of the trees in this scan, there is no barrel distortion in the radial scan. The trees scanned were also equidistant from the scanner due to the geometry of the radial scan allowing for even intensity across the scan. One of the disadvantages of radially scanning with the modBX scanner is that the scanning apparatus must be moved very slowly, on the order of .05m/s, in order to prevent the scanner from being jarred by sudden movements due to uneven ground.

## 4.2 Strawberries

Ground grown strawberries in Tampa, Florida were scanned using the handheld Mini-Z scanner. The Mini-Z scanner was held, pointed downward, about .5m above the plants and carried along a subsection of a row of plants.

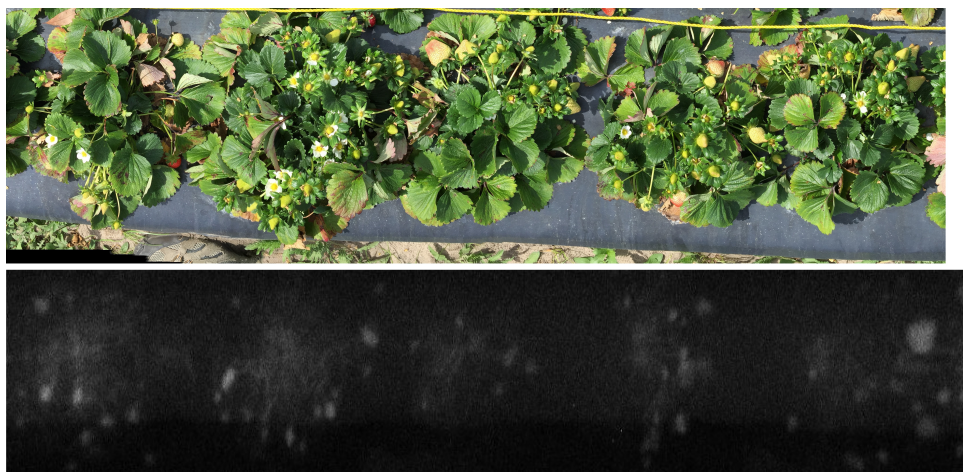


FIGURE 4.4: Scan and Photograph of Ground Planted Strawberries

As can be seen in the above image, many of the strawberries are fully obscured by the foliage of the plants in the photograph. The X-Ray beams successfully penetrated the upper foliage layer, allowing the backscatter image to reveal the underlying plant structure. In the backscatter image, the soil bundled in plastic that the strawberries are grown in, visible as black material in the photograph, appears as a hazy background in the upper half of the image.

## 4.3 Tomatoes

Trellis planted tomatoes in Naples, Florida were also scanned using the handheld Mini-Z scanner. In this situation the scanner was held approximately 10cm from the sides of the

tomato plants and was scanned vertically along individual plants, as well as horizontally along sections of the plant rows approximately 3m long.



FIGURE 4.5: Photograph of Trellis Planted Tomatoes. Courtesy of Lipman Produce.

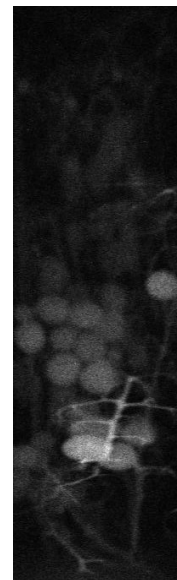


FIGURE 4.6: Vertical Scan of Tomato Plant

Trellis planted tomatoes have dense foliage cover and grow in rows with tightly intertwined plants. This makes seeing tomatoes growing on the plant with RGB cameras difficult. As was the case with apple trees and strawberry plants discussed earlier, the

X-Ray beam from the backscatter X-Ray machine was able to penetrate the outer foliage of the plant, revealing the inner plant structure and fruit.

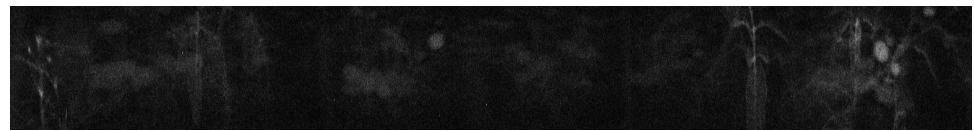


FIGURE 4.7: Horizontal Scan of Tomato Plants

## Chapter 5

# Sample Analysis of Image

In this chapter an algorithmic method of estimating crop yield of trellis planted apple trees will be explored. Raw images of the tree will be filtered. A method of detecting apple tree trunks will be discussed. This method was derived from methods used to detect ocular blood vessels with modifications made to better suit this application. [18] Pseudocode detailing the overall algorithm can be found in appendix A. [19]

## 5.1 Process overview

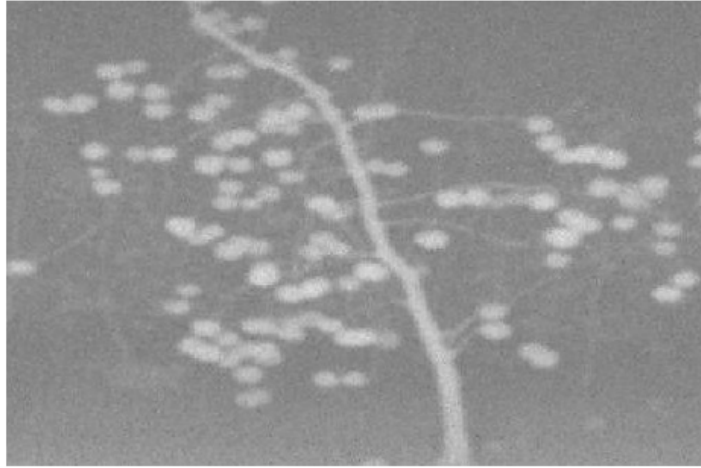


FIGURE 5.1: Scan of Apple Tree from ModBX Backscatter X-Ray Imager

### 5.1.1 Filtering Images

AS&E back-scatter X-Ray imagers have inbuilt signal processing algorithms that, due to their proprietary nature, will not be discussed in this paper. Although the images received from the devices are already pre-processed, because of the X-Ray backscatter imaging process, there is still a significant amount of salt and pepper noise present in the final images. One commonly accepted method of noise-removal used to deal with this type of noise in X-Ray images is median filtering. [20] As such, a 3px by 3px median filter is applied to the image before processing.

The median filter effectively eliminates some of the salt and pepper noise of the image, but this has the negative effect of softening the image overall by removing fine detail. Because we are interested primarily in the general location of the tree's trunk this is not a serious issue.

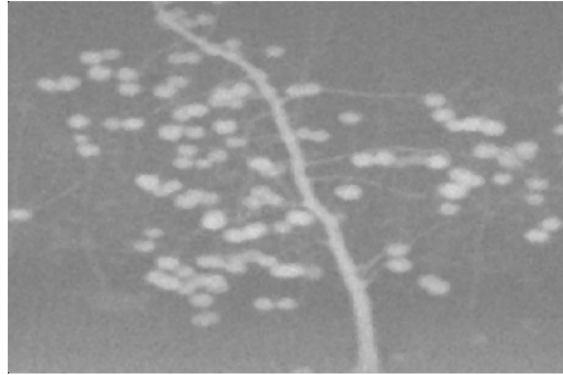


FIGURE 5.2: Scan After Application of Median Filter

Next, adaptive histogram equalization is applied to the image in order to increase the contrast in the image. As can be seen in figure 5.3 this causes the trunk and apples to stand out more readily from the background of the image.

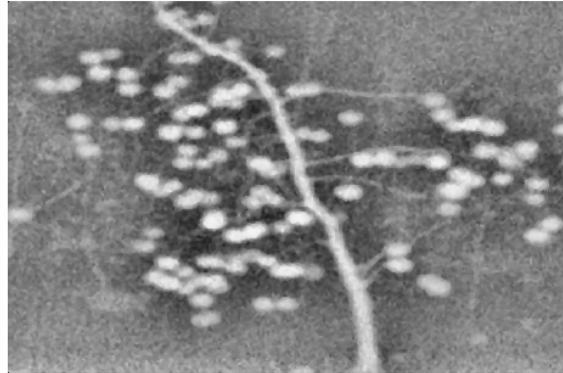


FIGURE 5.3: Adaptive Histogram Equalization

### 5.1.2 Processing Using Structured Elements

After filtering, the images are processed using morphological image processing to remove certain features of the image. [21] First, a circular 2d structured element is created with a radius about equal to the radius of an apple in the image and a magnitude of 1. Next,

a morphological opening is performed on the image in order to “find” apples within the image.

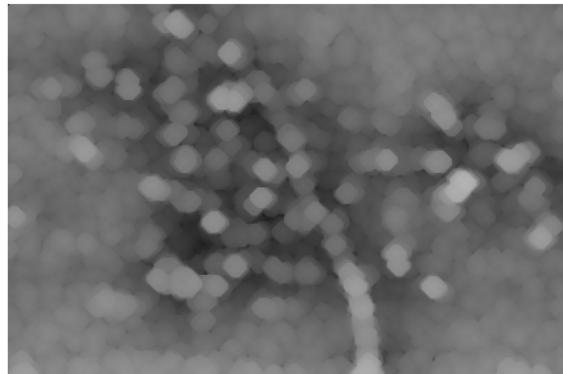


FIGURE 5.4: Morphological Opening

The morphological opening is then subtracted from the image in order to remove intensity in the scan that can be attributed to apples.

After this another larger circular 2d structured element is created in order to detect large clumps of apples that may still be left in the image. A morphological opening is then performed on the image and the result of this opening is once again subtracted from the image.

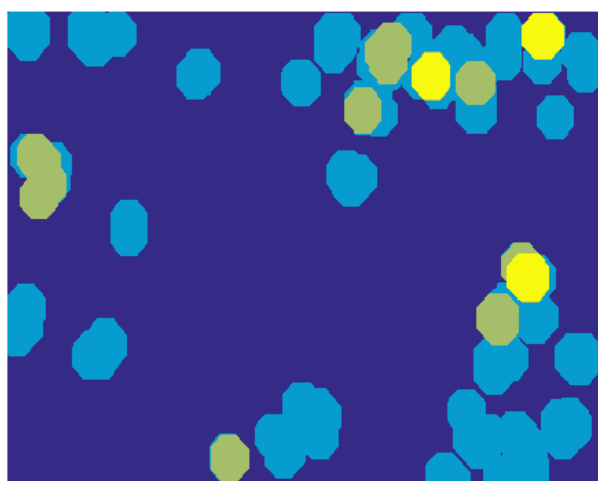


FIGURE 5.5: Second Morphological Opening

The intensity values of the image are then adjusted such that 1% of data is saturated at low and high intensity. This effectively readjusts the image values in order to restore contrast to the image after the morphological operations.

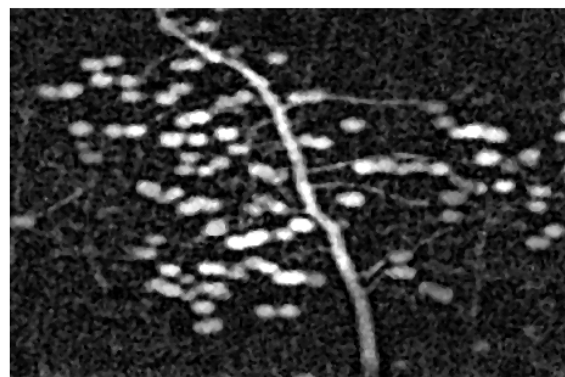


FIGURE 5.6: Image After Intensity Adjustment

### 5.1.3 Image Segmentation

After pre-processing the image, the image is segmented. A threshold value is selected using Otsu's method [22] and the image is binarized. Objects with areas less than 30px

are then removed from the image.



FIGURE 5.7: Binarized Image



FIGURE 5.8: Binarized Image with Objects Removed

Boundaries in the binarized image are then located using the Moore-Neighbor tracing algorithm modified by Jacob's stopping criteria [23]. Boundaries with lengths too small to be the trunk of the tree, less than 300 px, are removed. The remaining boundary represents the approximate trunk of the tree.

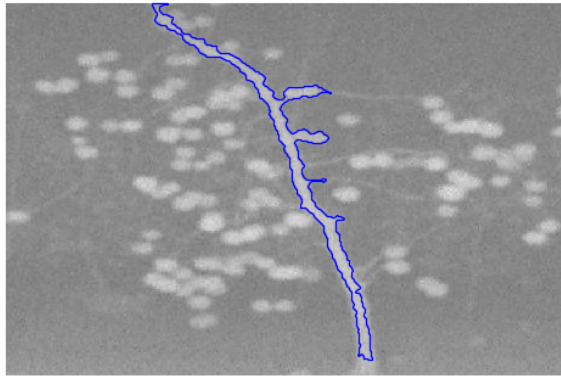


FIGURE 5.9: Trunk Boundary

#### 5.1.4 Using Path Planning to Locate the Trunk

In order to determine the location of the trunk within the trunk segment described above, a graph search method inspired by intelligent scissor segmentation is used. [24] [25]. The image is cropped to include only the area in which the trunk segment lies. This cropped image is smoothed using a 2d Gaussian kernel with a standard deviation of 2. Next a graph is created using the cropped image. First the image is inverted so that areas of high intensity correspond to low cost. Next the image is iterated through and a graph is created with one node for each pixel. Pixels are connected with the pixels immediately above, below and to the sides of themselves. The edges between these nodes are set to the average cost of the two pixels they are connecting. For example the edge connecting  $p_x$  and  $p_y$ ,  $E(p_x, p_y) = \frac{c(p_x) + c(p_y)}{2}$  where  $c(p_x)$  is the cost associated with  $p_x$ . The uppermost and lowermost points of the boundary surrounding the approximate tree trunk are then found. Using Dijkstra's algorithm, a shortest path between the uppermost and lowermost points of the boundary is found. [26] Due to the way in which the backscatter X-Ray imager generates images, the thickest area of the trunk will appear more intense on the scan than the outer edges of the trunk. By associating

higher intensity with lower cost, we can solve for the optimal path through the graph and thus find the path through the thickest area of the trunk.

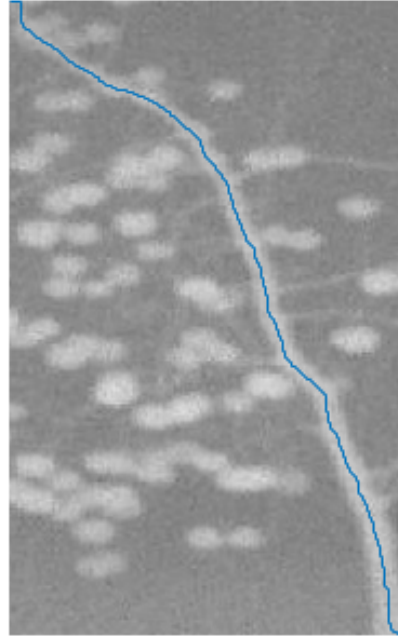


FIGURE 5.10: Optimal Path Through Trunk

After the path through the trunk is located, the average width of the trunk is estimated by determining the distance in pixels that one edge of the trunk boundary is from the opposing edge for each row of pixels in the image. The average of these distances is then calculated. The pixels to the right and left of the path are then set to an intensity of zero so that a band of intensities the width of the trunk is removed from the image. This can be seen as a black line in the image below.

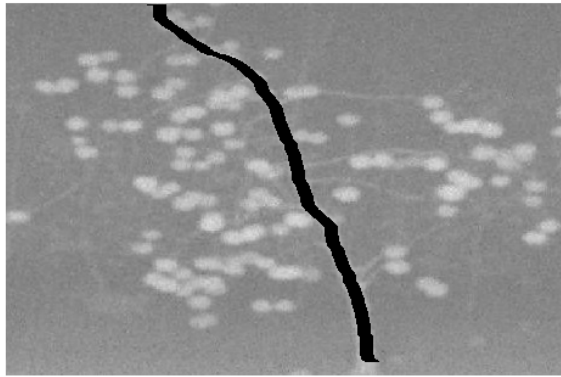


FIGURE 5.11: Scan With Trunk Removed

### 5.1.5 Determining Fruit Yield

With the intensity caused by the trunk of the tree removed from the image, the remaining intensity in the image can be attributed to three main factors; background noise, remaining plant structure, and fruit. The amount of remaining plant structure present in the scan is very small compared to the fruit and noise. Therefore, the sum of all intensity values across the image minus the sum of noise values across the image should be proportional to the agricultural yield present in the scan.

$$\sum_{k=1}^{numPixels} v(p_k) - n(p_k) \propto yield \quad (5.1)$$

Where  $v(p_k)$  is the intensity at pixel  $k$  and  $n(p_k)$  is the noise at pixel  $k$ .

# **Chapter 6**

## **Conclusions**

### **6.1 Overview**

In this paper we have reviewed the importance of precision agriculture in more sustainable and environmentally friendly agricultural activities. Firstly, an overview of the physics behind Compton Backscatter has been given. Second, the inner workings of a Compton Backscatter X-Ray imaging machine have been explored. Next, we viewed scans of trellis grown apple trees in Biglerville, PA, ground planted strawberries in Naples, FL, and trellis grown tomatoes in Naples, FL. Finally, an algorithmic method of estimating yield of apple trees was proposed.

### **6.2 Conclusions**

Overall, the scans of the apple, strawberry, and tomato plants look promising. Scans of the apple trees were clear and fruit were easy to differentiate from the background of the scans. In the scan of strawberry plants fruit can sometimes be difficult to discern

from other plant matter. The same can be said of the scans of the tomato plants, fruit can become difficult to discern from the background, especially in the horizontal scans. This may be able to be overcome in future scans via use of a Backscatter X-Ray imager with a more powerful beam. While in theory the proposed method of yield estimation should work, it is not possible to verify this without ground truth estimates of yield for individual apple trees.

### 6.3 Future Work

There are many ways in which the results of this paper can be expanded upon. More data must be collected with Backscatter X-Ray imagers along with ground truth yield estimates in order to show correlation between the intensity of fruit in the backscatter scans and yield. With enough data, machine learning approaches could be used to detect fruit in the scans, providing another way of estimating yield using Backscatter X-Ray imaging. [27] With improved scans from more powerful Backscatter X-Ray imagers, algorithmic image processing methods for determining yield could be developed for strawberries and tomatoes.

## Appendix A

# Image Processing Pseudocode

**Result:** I2

```
I ← readInImage('example.jpg');
medianFiltered ← medianFilter2d(I);
equalized ← adaptiveHistogramEqualize(medianFiltered);
open ← morphologicalOpen(equalized);
applesRemoved ← equalized - open;
medianFilteredApplesRemoved ← medianFilter2d(applesRemoved);
background ← morphologicalOpen(medianFilteredApplesRemoved);
I2 ← medianFilteredApplesRemoved - background;
I2 ← imageAdjustment(I2);
```

**Algorithm 1:** Image Pre-processing

**Result:** b

```
level ← OtsuThreshold(I2);  
bw ← binarize(I2,level);  
bw ← removeSmallObjects(bw);  
boundaries ← findBoundaries(bw)  
for  $k = 1$  to  $\text{numberOfElementsIn}(b)$  do  
    if  $b(k) < \text{threshold}$  then  
        | Remove  $b(k)$  from b;  
    end  
end
```

**Algorithm 2:** Segmentation

**Result:** yield

```
bottom ← findBottom(b);  
top ← findTop(b);  
inverted ← invert(I2);  
blurred ← gaussianBlur(inverted);  
graph ← imageToGraph(blurred);  
path ← Dijkstra(graph,bottom,top);  
width ← findAverageTrunkWidth(b);  
for  $i = 1:path.length$  do  
     $I(path(i,1), path(i,2)-(width/2):path(i,2)+(width/2)) \leftarrow 0;$   
end  
yield ← 0;  
for all pixels in  $I$  do  
    yield ← yield + pixelInI - perPixelNoise;  
end
```

**Algorithm 3:** Segmentation

# Bibliography

- [1] Oxford Instruments. Typical X-ray Spectra by Anode Material. Technical report, Oxford Instruments X-Ray Technology, 360 El Pueblo Road, Suite 104 Scotts Valley, CA 95066 USA, 03 2015.
- [2] Philip R. McLoud and Ron Gronwald. Precision agriculture: Nrcs support for emerging technologies. *stelprdb1043474.pdf*, Jun 2007. URL [http://www.nrcs.usda.gov/internet/fse\\_documents/stelprdb1043474.pdf](http://www.nrcs.usda.gov/internet/fse_documents/stelprdb1043474.pdf).
- [3] Michael Robertson, Peter Carberry, and Lisa Brennan. The economic benefits of precision agriculture: case studies from australian grain farms. 2007.
- [4] Specialty crops- an overview. URL <http://nationalaglawcenter.org/overview/specialty-crops/>.
- [5] What is a specialty crop?, 2014. URL <https://www.ams.usda.gov/services/grants/scbgp/specialty-crop>.
- [6] What is horticulture? URL <http://www.ashs.org/?page=horticulture>.
- [7] Rich Marini. Estimating apple yield and fruit size, Dec 2013. URL <http://extension.psu.edu/plants/tree-fruit/news/2013/estimating-apple-yield-and-fruit-size>.
- [8] Bruno Basso, Davide Cammarano, and Elisabetta Carfagne. Review of crop yield forecasting methods and early warning systems. URL [http://www.fao.org/fileadmin/templates/ess/documents/meetings\\_and\\_workshops/gs\\_sac\\_2013/improving\\_methods\\_for\\_crops\\_estimates/crop\\_yield\\_forecasting\\_methods\\_and\\_early\\_warning\\_systems\\_lit\\_review.pdf](http://www.fao.org/fileadmin/templates/ess/documents/meetings_and_workshops/gs_sac_2013/improving_methods_for_crops_estimates/crop_yield_forecasting_methods_and_early_warning_systems_lit_review.pdf).

- [9] Stephen T. Nuske, Stephen Kyle Wilshusen, Supreeth Achar, Luke Yoder, Srinivas G Narasimhan, and Sanjiv Singh. Automated visual yield estimation in vineyards. *Journal of Field Robotics*, 31(5):837–860, September 2014.
- [10] D. Stajnko, M. Lakota, and M. Hocevar. Application of thermal imaging for visualization of high density orchards and counting apple fruits. *Acta Hortic. Acta Horticulturae*, (707):211215, 2006. doi: 10.17660/actahortic.2006.707.26. URL [http://www.actahort.org/books/707/707\\_26.htm](http://www.actahort.org/books/707/707_26.htm).
- [11] Compton scattering, Apr 2016. URL <http://www.merriam-webster.com>.
- [12] John David Jackson. *Classical electrodynamics*. John Wiley & Sons, Inc., 1962.
- [13] NDT Education Resource Center. X-rays, 2014. URL <https://www.nde-ed.org/educationresources/communitycollege/radiography/physics/xrays.htm>.
- [14] S.W. Smith. X-ray backscatter detection system, January 19 1993. URL <http://www.google.com/patents/US5181234>. US Patent 5,181,234.
- [15] P. Rothschild, J. Schubert, W. Baukus, W. Sapp, R. Schueller, J. Callerame, and W. Cason. X-ray inspection based on scatter detection, May 3 2007. URL <https://www.google.com/patents/US20070098142>. US Patent App. 11/551,991.
- [16] Mini z, 2016. URL <http://as-e.com/products-solutions/cargo-vehicle-inspection/handheld-inspection-2/product/mini-z/>.
- [17] Mini z handheld z backscatter screening system, 2014. URL <http://www.easterncommunications.com/wp-content/uploads/2014/08/MINI-Z-Data-Sheet.pdf>.
- [18] Tyler Coye. A novel retinal blood vessel segmentation algorithm for fundus images. *A Novel Retinal Blood Vessel Segmentation Algorithm for Fundus Images*, Dec 2015. URL <http://www.mathworks.com/matlabcentral/fileexchange/50839-a-novel-retinal-blood-vessel-segmentation-algorithm-for-fundus-images>.
- [19] Patwari Manjiri, Manza Ramesh, Rajput Yogesh, Saswade Manoj, and Deshpande Neha. Automated localization of optic disk, detection of microaneurysms and extraction of blood vessels to bypass angiography. *Advances in Intelligent Systems*

- and Computing Proceedings of the 3rd International Conference on Frontiers of Intelligent Computing: Theory and Applications (FICTA) 2014, page 579587, 2015. doi: 10.1007/978-3-319-11933-5\_65.
- [20] Rafael C. Gonzalez and Richard E. Woods. *Digital image processing*. Prentice Hall, 2002.
- [21] Edward R. Dougherty and Roberto A. Lotufo. *Hands-on morphological image processing*. SPIE Optical Engineering Press, 2003.
- [22] Nobiyuki Otsu. A threshold selection method from gray-level histograms. *IEEE Transactions on Systems, Man, and Cybernetics IEEE Trans. Syst., Man, Cybern.*, 9(1):6266, 1979. doi: 10.1109/tsmc.1979.4310076.
- [23] Rafael C. Gonzalez, Richard E. Woods, and Steven L. Eddins. *Digital Image processing using MATLAB*. Dorsing Kindersley, 2004.
- [24] Eric N. Mortensen and William A. Barrett. Intelligent scissors for image composition. *Proceedings of the 22nd annual conference on Computer graphics and interactive techniques - SIGGRAPH '95*, 1995. doi: 10.1145/218380.218442. URL <http://courses.cs.washington.edu/courses/csep576/15sp/readings/mort-sigg95.pdf>.
- [25] D. Geiger, A. Gupta, L.a. Costa, and J. Vlontzos. Dynamic programming for detecting, tracking, and matching deformable contours. *IEEE Transactions on Pattern Analysis and Machine Intelligence IEEE Trans. Pattern Anal. Machine Intell.*, 17(3):294302, 1995. doi: 10.1109/34.368194.
- [26] Kurt Mehlhorn and Peter Sanders. *Algorithms and data structures: the basic toolbox*. Springer, 2008.
- [27] Kyosuke Yamamoto, Wei Guo, Yosuke Yoshioka, and Seishi Ninomiya. On plant detection of intact tomato fruits using image analysis and machine learning methods. *Sensors*, 14(7):1219112206, Sep 2014. doi: 10.3390/s140712191. URL <http://www.ncbi.nlm.nih.gov/pmc/articles/pmc4168514/>.